DNA Oxidation by Charge Transport in Mitochondria†

Edward J. Merino and Jacqueline K. Barton*

Division of Chemistry and Chemical Engineering, California Institute of Technology, Pasadena, California 91125

Received August 30, 2007; Revised Manuscript Received November 20, 2007

ABSTRACT: Sites of oxidative DNA damage in functioning mitochondria have been identified using a rhodium photooxidant as a probe. Here we show that a primer extension reaction can be used to monitor oxidative DNA damage directly in functioning mitochondria after photoreaction with a rhodium intercalator that penetrates the intact mitochondrial membrane. The complex $[Rh(phi)_2bpy]Cl_3$ (phi = 9,10-phenanthrenequinonediimine) binds to DNA within the mitochondria and, upon irradiation, initiates DNA oxidation reactions. Significantly, piperidine treatment of the mitochondria leads to protein-dependent primer extension stops spaced every ∼20 base pairs. Hence, within the mitochondria, the DNA is well covered and packaged by proteins. Photolysis of the mitochondria containing $[Rh(phi)_2bpy]^{3+}$ leads to oxidative DNA damage at positions 260 and 298; both are mutational hot spots associated with cancers. The latter position is the 5′-nucleotide of conserved sequence block II and is critical to replication of the mitochondrial DNA. The oxidative damage is found to be DNA-mediated, utilizing a charge transport mechanism, as the Rh binding sites are spatially separated from the oxidation-prone regions. This long-range DNA-mediated oxidation occurs despite protein association. Indeed, the oxidation of the mitochondrial DNA leads not only to specific oxidative lesions, but also to a corresponding change in the protein-induced stops in the primer extension. Mitochondrial DNA damage promotes specific changes in protein−DNA contacts and is thus sensed by the mitochondrial protein machinery.

Mitochondria (mt) are thought to play an essential role in cancerous transformation (*1*, *2*). The mt of many tumor cells do not produce a potential energy gradient (*3*). Additionally, a variety of mutations have been detected within mt genomes of tumor cells (*4*−*6*). Many such mutations have been localized to the control region of mt in conserved sequence block II (*7*, *8*).

Much work has gone into understanding the role of oxidative phosphorylation in the generation of mutation-prone nucleotide analogues, especially 8-oxo-deoxyguanosine (*9*, *10*). Importantly, a sequence level view of DNA damage in functioning mt has been limited by several technical issues. Most experiments utilize either ligation-mediated PCR (*11*) or an approach that measures alterations at a small subset of nucleotides (*12*). We have recently reported that detection of DNA lesions made by an exogenous oxidant can be accomplished by simple primer extension (*13*). This methodology now provides an opportunity to examine and to compare oxidative DNA damage in vivo and in vitro.

Rhodium intercalators that contain the phenanthrenquinonediimine (phi) ligand are employed to generate oxidative damage in DNA (*14*). With photoactivation, these rhodium intercalators promote one-electron oxidation of DNA. Upon photoactivation of $[Rh(phi)_2bpy]^{3+}$ at ∼320 nm, direct cleavage of the sugar phosphate backbone at the site of intercalation is observed (*15*). Importantly, the phi intercalator also couples the Rh oxidant into the DNA base stack (*16*) to facilitate base oxidation over direct cleavage of the sugar phosphate backbone when lower energy irradiation at 365 nm is used. We first demonstrated oxidative damage from a distance (*16*) using phi complexes of rhodium tethered to the end of an oligonucleotide and spatially separated from guanine doublets in DNA; the 5′-guanines of guanine doublets and triplets are sites of particularly low oxidation potential (*17*). When larger regions of DNA are surveyed, a covalent phi complex cannot be tethered to the DNA but instead noncovalent $[Rh(phi)_2bpy]^{3+}$ can be employed. By distinguishing between those strand breaks that result from high-energy irradiation, marking rhodium binding sites, versus lower energy irradiation, marking sites of one-electron oxidation, one can therefore identify damage to DNA that must arise from a distance by charge transport.

Our laboratory has explored the chemistry of DNA-mediated charge transport and its biological consequences (*18*, *19*). We have shown that one-electron oxidative damage to DNA can arise from a distance as a result of hole migration through the DNA base pair stack (*16*, *20*). Remarkably, oxidative DNA damage can occur at least 200 Å away from the site of oxidant binding (*20*), and thus, its biological consequences require consideration. Long-range oxidative damage has been demonstrated both in nucleosomes (*21*, *22*) and within cell nuclei (*23*). We are interested here in determining whether DNA oxidative damage is localized to biologically important sites in mt genomes, the source of much oxidative stress in the cell (*24*).

Previously, we identified oxidation-prone regions on bare mtDNA that result from the funneling of one-electron

† We are grateful to the NIH (Grant GM49216) for their financial support of this research including a minority postdoctoral fellowship to E.J.M.

* To whom correspondence should be addressed. E-mail: jkbarton@caltech.edu. Phone: (626) 395-6075. Fax: (626) 577-4976.

10.1021/bi701775s CCC: $40.75
Published on Web 01/12/2008

damage by long-range charge transport (*13*). The damage is funneled to an important regulatory element, conserved sequence block II, and overlaps with hot spots for mutation. We were interested in understanding whether differences in DNA oxidation would arise in the complex environment of functioning mt, since in the mt, DNA is bound by proteins and packaged (*25*). In this work, we show the ability of $[Rh(phi)_2bpy]^{3+}$ to penetrate mt and damage mtDNA. We show that the $[Rh(phi)_2bpy]^{3+}$-induced damage pattern is highly similar to that of bare mtDNA and results from long-range charge transport despite the association of the DNA with proteins. In fact DNA oxidation is found to alter protein−DNA contacts.

MATERIALS AND METHODS

All experiments were carried out using HeLa cells. HeLa cells (Sigma) were raised to ~75% confluence, trypsinized, and washed twice with PBS. The cells were then homogenized (Mitochondrial Isolation Kit, Sigma) using a modified procedure. The cells (50 million) were suspended in freshly prepared extraction buffer (6 mL, pH 7.5, 10 mM Hepes, 200 mM mannitol, 70 mM sucrose, 1 mM EGTA) for 5 min at 4 °C. The cells were then homogenized with 10 strokes in a 3 mL glass tube with a plastic pestle. Samples were pooled, aliquoted (5 million cells), and centrifuged for 10 min at 4 °C. The supernatant was removed, and each sample was resuspended in storage buffer (200 μL; 10 mM Hepes, pH 7.5, 250 mM sucrose, 1 mM ATP, 0.8 mM ADP, 5 mM sodium succinate, 2 mM potassium phosphate, 1 mM DTT). An appropriate amount of $[Rh(phi)_2bpy]Cl_3$ was dissolved in storage buffer and added to the cells. All cells were then incubated at 37 °C in the dark for 30 min. Determination of functioning mt was carried out according to protocol (Mitochondrial Isolation Kit) utilizing purified mt rather than homogenized cells. Spectra were normalized to the 525 nm emission.

Oxidation of DNA in functioning mt was carried out by irradiation for 30 min at 37 °C using a solar simulator (Orion) outfitted with an additional glass filter that helps eliminate wavelengths below 345 nm. For studies involving direct DNA strand cleavage, the additional glass filter was removed. The samples were incubated with 99% piperidine (20 μL, 10 min, 95 °C) and cooled, and 20 μL of glacial acidic acid was added. The sample was prepared for primer extension by purification with DNeasy Tissue Kit (QIAquick, Qiagen) using a modified procedure. Cell lysis buffer (240 μL, guanidinium chloride) was added to the neutralized samples without additional proteinase K, purified as described by the manufacturer, and eluted into 100 μL. Primer extension was carried out by adding 30 μL of this mix to a 2× primer extension mix (2× Vent buffer, 200 μM dNTP, 1 μM ^{32}P-end-labeled primer, and 0.2 U/μL Platinum Taq). Extensions were carried out by heating to 95 °C for 2.5 min and cycled 40 times (55 °C for 40 s, 72 °C for 40 s, 95 °C for 30 s). The samples were precipitated, and 6% denaturing PAGE was performed. The gels were visualized by overnight exposure to a phosphorImager screen and scanned. Agarose gel analysis was done by adding 18 μL of DNA purified after piperidine treatment with 3 μL of 50% glycerol with bromophenol blue. Oxidation experiments on bare DNA were carried out in a manner similar to that described (*13*) using Taq polymerase.

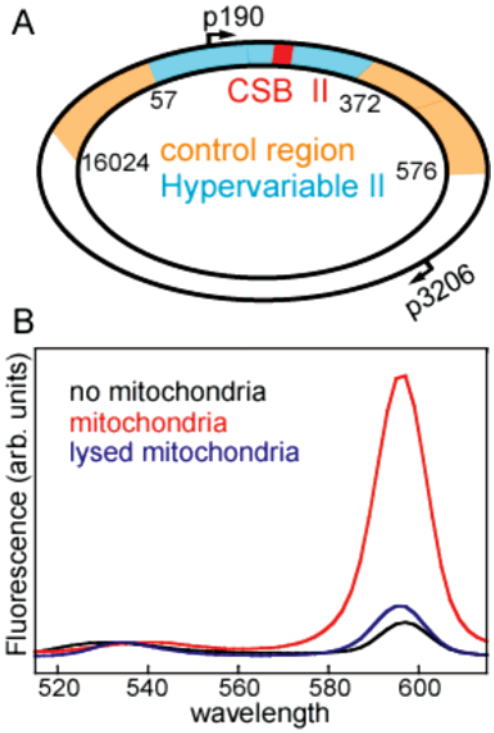

FIGURE 1: Assays for damage in functioning mitochondria. (A) The mitochondrial genome contains the noncoding control region (orange, nucleotides 16024−576). Regulation of DNA replication and transcription occurs in the hypervariable region (blue, nucleotides 57−372) within a conserved sequence block (red, 299−315). $[Rh(phi)_2bpy]^{3+}$-induced oxidation was determined using p190 that overlaps with the conserved sequence block. The primer p3206 was also utilized. (B) Addition of the dye JC-1 to homogenized mitochondria (red) gives high fluorescence at 590 nm, indicating that the mitochondria are functional. Less fluorescence is observed when no mitochondria (black) are present or when mitochondria are completely lysed (blue).

Primer p190 is 5′-gcacctacgttcaatattacaggcgaac, and p3206 is 5′-gatatcatctcaacttagtattataccc. For manual sequencing, the control region and a region including nucleotides 3123−3870 were amplified by PCR by using appropriate primers. After purification, sequencing reactions were accomplished by addition of acyclo-dNTP [1× Vent buffer, 100 μM dNTP, 66 μM acyclonucleotide, 3 μM ^{32}P-end-labeled primer, 10 U Vent(exo$^-$)] and cycled as listed above. The data were quantified using the line function in ImageQuant (Amersham) and normalized in Excel.

RESULTS

Primer Extension of DNA from Functioning Mitochondria. In this study we used two primers, p190 and p3206, which are named for the mt position of the 3′-nucleotide (Figure 1). In contrast to ligation-mediated PCR, primer extension permits the visualization of DNA lesions generated in vivo in a few hours. Figure 2 shows the strategy we employed. HeLa cells (5 million) were raised to 75−90% confluence, trypsinized, and homogenized to facilitate $[Rh(phi)_2bpy]^{3+}$ incorporation into mt. Addition of 15−75 μM $[Rh(phi)_2bpy]^{3+}$ at 37 °C causes mt and other cellular components to turn orange, an indication that $[Rh(phi)_2bpy]^{3+}$ traverses the mt membrane.

We evaluated the functioning of mt using JC-1, a cationic fluorophore, as a reporter (*26*). Addition of JC-1 to a buffered

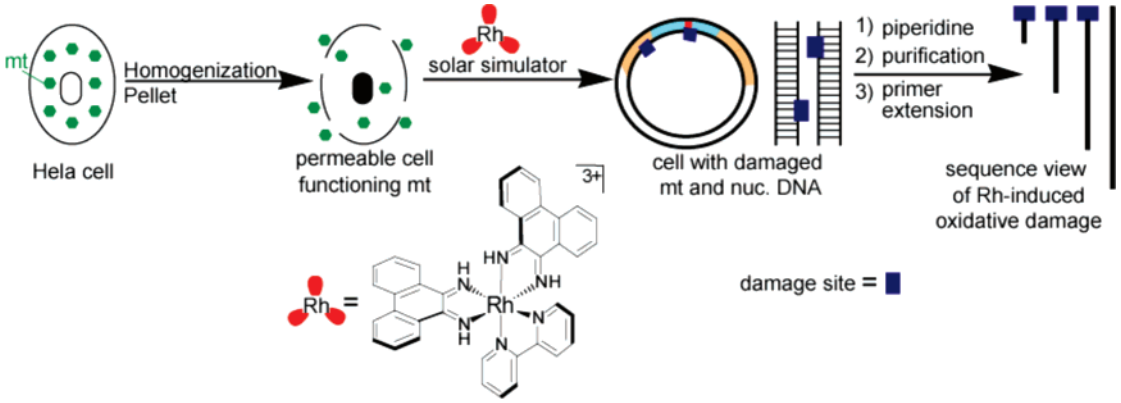

FIGURE 2: Schematic illustration of the strategy to detect oxidative damage to functioning mt with the Rh photooxidant. HeLa cells were homogenized to facilitate $[Rh(phi)_2bpy]^{3+}$ incorporation into mitochondria. Irradiation induces DNA oxidation (blue squares). After workup, the sites of oxidation can be interrogated via primer extension assay.

solution yields the expected spectrum containing both monomer and dye aggregates (Figure 1B, black spectrum) centered at 525 and 590 nm, respectively. Because of the potential energy gradient generated in functioning mt, JC-1 enters mitochondria and subsequently aggregates. As a result, addition of fractionated mt causes an increase in the 590 nm emission, reflecting JC-1 aggregation due to transport inside the mt because of the gradient (Figure 1B, red spectrum). Emission at 590 nm is not evident with overhomogenization, where all membranes are ruptured (Figure 1B, blue spectrum). Spectra of the homogenized whole cells give results similar to those observed with functioning mitochondria; in this case dye aggregates could be dependent on increased dye concentration within the homogenized cell membrane (data not shown).

Faithful primer extension requires processing of the mtDNA. Previously, we reported that a sufficient signal could be visualized with as little as 4 μg of total HeLa DNA, 10 fmol in mtDNA, if the mtDNA were restricted by *Eco*RI (*13*). Because cellular DNA fractions are damaged in the presence of $[Rh(phi)_2bpy]^{3+}$, a restriction approach is not reliable: the enzyme may exhibit lower specificity or be inhibited. Without restriction, to achieve high signals of primer extension of the isolated mtDNA, a piperidine treatment at 95 °C was utilized. MtDNA exists as closed circular, supercoiled DNA. Piperidine nicks the mtDNA backbone at damaged sites, facilitating relaxation from the supercoiled form and melting of the duplex to aid in the annealing of the primer.

Piperidine can be added before or after purification of DNA from proteins and other cellular components. Extending p190 on a total HeLa DNA sample that has been purified and then piperidine-treated gives a large high molecular weight product (Figure 3). The wide product distribution is indicative of uninterrupted extension limited by the polymerization time. Most interestingly, addition of piperidine before DNA purification leads instead to a repetitive primer extension stop pattern spaced ~15−20 base pairs. The stop pattern begins to coalesce to give a shorter size product than that obtained when total HeLa DNA is purified prior to piperidine treatment. Within the initial 80 base pairs, 7 discrete stops can be visualized.

We then tested whether these stops were specific to the control region or to the area surrounding p190 of the mtDNA genome; p3206 is far removed from p190 and is not within

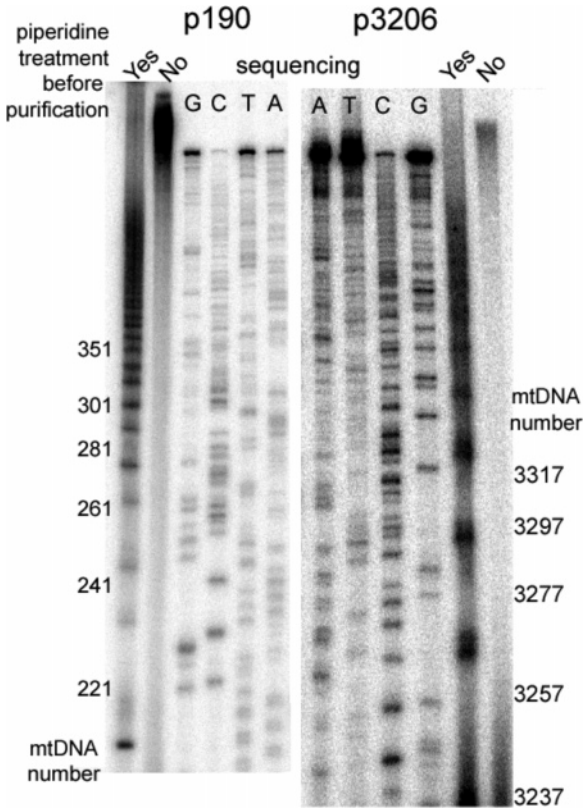

FIGURE 3: Primer extensions utilizing piperidine to monitor protein-dependent DNA stops. Two primers, one inside (p190, left side) and one outside (p3206, right side) the control region, were extended on DNA samples that were piperidine treated before and after DNA purification. Piperidine treatment after purification gives a good yield with no stops (lane marked "NO") because piperidine removes supercoiling and melts DNA strands. In contrast, addition of piperidine to functioning mitochondria causes protein-related stops during the primer extension reaction. These stops are visualized by both primers even though they interrogate positions 3000 base pairs apart.

the mtDNA control region. Purification of DNA, piperidine treatment, and extension of p3206 leads to a high molecular weight product similar in length to that observed with p190. Treatment with piperidine prior to DNA purification leads also to a primer extension stop pattern. The stop pattern is less frequent, with only 3 stops visualized within the first 80 base pairs. Addition of proteinase K leads to removal of this primer extension stop pattern (Supporting Information Figure 1). Because the stop pattern is removed by treatment

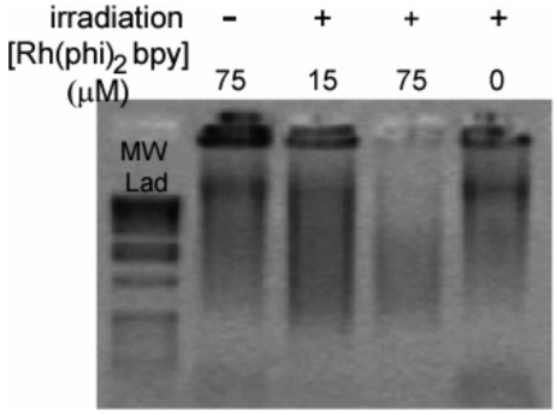

FIGURE 4: Agarose gel analysis of oxidized HeLa DNA. DNA from functioning mitochondria were irradiated in the absence of [Rh(phi)$_2$bpy]$^{3+}$ or were treated with [Rh(phi)$_2$bpy]$^{3+}$ without irradiation. These lanes show only high molecular weight products. Addition of [Rh(phi)$_2$bpy]$^{3+}$ (15 or 75 μM) gives DNA products of lower molecular weight, indicating that [Rh(phi)$_2$bpy]$^{3+}$ traverses the mitochondrial membrane and oxidized DNA, creating strand breaks after piperidine treatment.

with guanidinium chloride (in the DNA purification protocol) or proteinase K, these primer extension stops appear to be protein-related.

Oxidative Damage to DNA in Functioning Mitochondria. The primer extension method allows us to determine the sequence dependence of oxidative DNA damage generated by Rh photolysis in functioning mt compared to bare DNA treated with Rh in the absence of proteins or other components from the mt. We first explored conditions for optimum uptake of [Rh(phi)$_2$bpy]$^{3+}$ into the mt. For optimization, piperidine-treated, single-stranded HeLa DNA samples were examined using agarose gel electrophoresis. Incubation of homogenized HeLa with [Rh(phi)$_2$bpy]$^{3+}$ in the absence of light or irradiation of homogenized cells without [Rh(phi)$_2$bpy]$^{3+}$ causes a large molecular weight DNA product as visualized by ethidium bromide staining (Figure 4). Incubation of the homogenized cells with 75 μM [Rh(phi)$_2$bpy]$^{3+}$ followed by irradiation leads to a decrease in the average molecular weight, indicative of oxidative damage and subsequent piperidine-dependent strand cleavage. Incubation with 15 μM [Rh(phi)$_2$bpy]$^{3+}$ causes a much wider distribution of both high and lower molecular weight products similar to a mixture of unmodified DNA and DNA with oxidative damage. Subsequent experiments utilize a Rh concentration of 15−45 μM. These data indicate that [Rh(phi)$_2$bpy]$^{3+}$ can traverse the mt membrane, bind DNA, and initiate oxidative photoreactions within functioning mt.

Under conditions that permit [Rh(phi)$_2$bpy]$^{3+}$-induced oxidative damage of mtDNA, the sequence details were investigated with p190. As before, incubation of homogenized HeLa with [Rh(phi)$_2$bpy]$^{3+}$ alone or with irradiation of the homogenized cells without [Rh(phi)$_2$bpy]$^{3+}$ causes the same protein-related stop pattern upon primer extension (Figure 5A) as homogenized HeLa (Figure 3). Therefore, no sequence-dependent damage to mt is caused by irradiation without Rh or incubation with [Rh(phi)$_2$bpy]$^{3+}$ without light. Upon addition of [Rh(phi)$_2$bpy]$^{3+}$ followed by irradiation, we observe increases in the primer extension stop pattern, attributed to new oxidative lesions, and decreases in the primer extension stop pattern, attributed to the removal of protein-related primer extension stops. The changes to the primer extension stop pattern are dependent on the concentration of [Rh(phi)$_2$bpy]$^{3+}$, with the increases and decreases changing proportionally. The major sites of oxidative damage by Rh occur at positions 220, 260, and 298, with parallel decreases in stop sites evident at 225, 266, and 302. The sequences associated with the oxidative lesions or damage sites (complementary to the sequence of the primer used) are 5′-AAGCATT, 5′-GTGGCTG, and 5′-G$_7$AAAGG.

A comparison between the sites with increased cleavage in functioning mt and those on bare DNA shows a correlation between locations of DNA damage induced by [Rh(phi)$_2$bpy]$^{3+}$ (Figure 5B). Two of the sites, at positions 260 and 298, are well correlated to sites that are prone to damage via base oxidation by charge transport (Figure 5B, red and black lines). These sites, as indicated previously in characterizing oxidative damage on naked mitochondrial DNA, correspond to guanine tracts and represent sites of low oxidation potential (*13*). The increase at position 220 is close to a [Rh(phi)$_2$bpy]$^{3+}$ binding site (Figure 5B; compare red and olive lines). The small but consistent two base pair shift versus that seen with bare mtDNA in the position of damage is likely due to the difference in Vent and Taq polymerase recognizing the piperidine-cleaved DNA-damaged products, with Vent polymerase recognizing the 3′-glycol from piperidine treatment and halting extension.

Next, we ascertained whether the [Rh(phi)$_2$bpy]$^{3+}$-induced damage sites occur via base oxidation by a charge transport mechanism. The external filter of the light source was removed, allowing wavelengths between 320 and 400 nm into the sample; piperidine was not added since it is not required to reveal direct strand cleavage by Rh at high energy. Under these conditions, an 8-fold loss in signal is observed, but the signal is still discernible above the background (Figure 6). As a reference, functioning mt were treated with [Rh(phi)$_2$bpy]$^{3+}$, irradiated, and piperidine-treated to give a similar primer extension stop pattern but with new peaks evident also corresponding to [Rh(phi)$_2$bpy]$^{3+}$ binding sites (Figure 6; compare black line to Figure 5). Without piperidine treatment, incubation of homogenized HeLa with [Rh(phi)$_2$bpy]$^{3+}$ alone (data not shown) or irradiation of the homogenized cells without [Rh(phi)$_2$bpy]$^{3+}$ (Figure 6, blue line) causes a large molecular weight product to be observed. Addition of [Rh(phi)$_2$bpy]$^{3+}$ and irradiation without piperidine treatment also yield a large molecular weight product accompanied by an observable damage pattern that is similar to that of the piperidine-treated samples, but with one key difference: several of the peaks are noticeably higher in peak height with piperidine treatment (compare peaks in piperidine-treated and non-piperidine-treated samples). Base oxidation promotes strand cleavage only with piperidine treatment, and thus, sites of base oxidation are of higher intensity by this method. Positions 260 and 298 are therefore assigned to sites of base oxidation, while position 220 is not. Furthermore, three locations, positions 218, 225, and 253, are identified as binding sites for [Rh(phi)$_2$bpy]$^{3+}$. Since these sites of base oxidation by [Rh(phi)$_2$bpy]$^{3+}$ (positions 260 and 298), which correspond to sites of low oxidation potential, do not overlap sites of [Rh(phi)$_2$bpy]$^{3+}$ binding, these data indicate that one-electron base oxidation of DNA is a consequence of long-range charge transport within functioning mt.

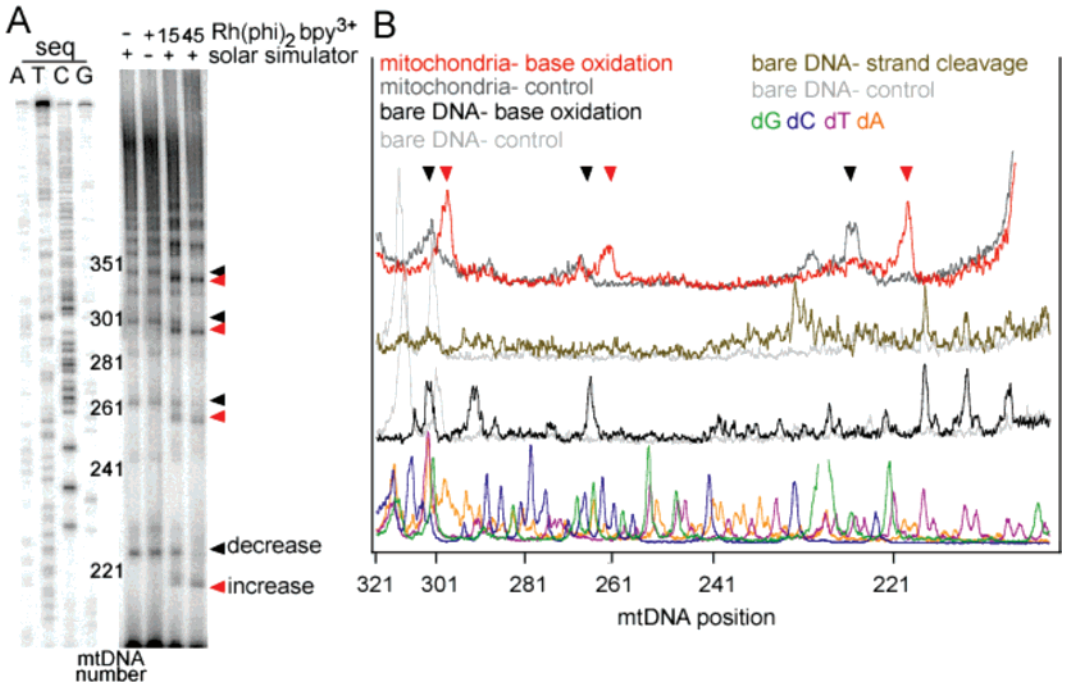

FIGURE 5: $[Rh(phi)_2bpy]^{3+}$-induced oxidation in functioning mitochondria. (A) In control experiments, primer extension of DNA from functioning mitochondria, where the oxidant $[Rh(phi)_2bpy]^{3+}$ is omitted or no irradiation occurs, shows no change in the protein-related stop pattern. Addition of 15 μM $[Rh(phi)_2bpy]^{3+}$ causes new primer extension products (red triangles), which correspond to sites that are oxidized and subsequently cleaved with piperidine treatment. A greater extent of DNA lesion formation can be visualized by increasing the Rh photooxidant concentration to 45 μM. A decrease in intensity is observed near DNA damage sites (black triangles). (B) Line plot of $[Rh(phi)_2bpy]^{3+}$-induced oxidative damage in functioning mitochondria (red), base oxidation of purified DNA (olive), and direct strand cleavage of purified DNA at Rh binding sites (black). For reference, sequencing lanes are plotted (various colors). Two sites of oxidative damage in functioning mitochondria, positions 260 and 298, overlap with sites of base oxidation on bare DNA. The third site, position 220, overlaps with a Rh binding site.

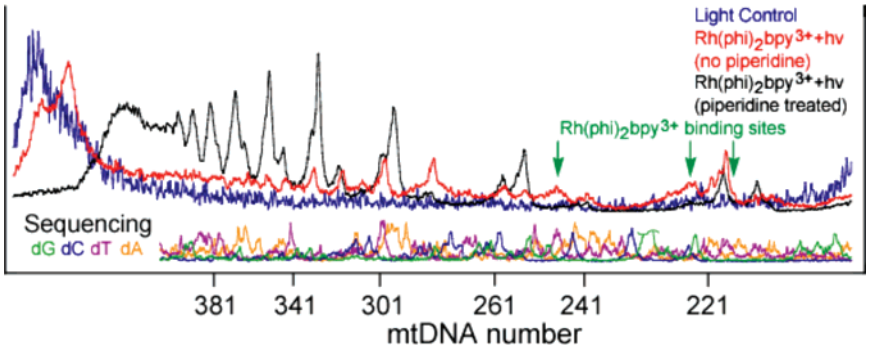

FIGURE 6: DNA oxidation by long-range charge transport. Line plots of primer extension products generated by irradiation with 320−400 nm light to induce both strand scission at Rh binding sites and one-electron base oxidation. Irradiation without $[Rh(phi)_2bpy]^{3+}$ causes a large molecular weight product with no DNA damage (blue). Addition of $[Rh(phi)_2bpy]^{3+}$ and treatment with piperidine causes both base oxidation and direct strand cleavage at Rh binding sites (black). Comparison to a similar sample that has not been treated with piperidine shows sites where $[Rh(phi)_2bpy]^{3+}$ binds (red). The sites of binding are at positions that do not increase in intensity upon piperidine treatment (green arrows).

DISCUSSION

Probing Sites of DNA Oxidation in Mitochondria with Rhodium. We have found that primer extension can be used to probe oxidative DNA damage directly in functioning mt. Piperidine treatment of mt was found to induce protein-dependent primer extension stops that are removed by denaturants or proteinase K. With $[Rh(phi)_2bpy]^{3+}$ oxidation, we find bands that either increase (due to the formation of DNA lesions) or decrease (due to the removal of protein-induced stops), and these increases and decreases are correlated with one another. Although the data in functioning mt are more complex than for bare mtDNA, these sites of oxidative damage are similar to sites previously observed on bare DNA. These DNA damage sites correspond to sites with high guanosine content, known positions of low oxidation potential (*17*).

Utilizing $[Rh(phi)_2bpy]^{3+}$ as an oxidant has several advantages compared to addition of peroxide, which is typically utilized to induce oxidative lesions in cells (*1*). The rhodium intercalator preferentially targets duplex DNA. Peroxides, instead, are nonspecific and react also with proteins, lipids, and other cellular components. Thus, analysis based upon peroxide treatment is convoluted by damage to these other components. Furthermore, $[Rh(phi)_2bpy]^{3+}$ irradiation conditions allow one to distinguish between sites of Rh binding and base oxidation.

Funneling Oxidative Damage to Specific Sites by Charge Transport. DNA oxidation is seen to occur through DNA-mediated charge transport since the $[Rh(phi)_2bpy]^{3+}$ binding sites do not overlap with oxidation sites. Oxidative damage is therefore being funneled within the mitochondrion to specific sites of low oxidation potential.

Charge transport may play a general role in generating DNA damage in mitochondria. Here irradiation of $[Rh(phi)_2bpy]^{3+}$ at long wavelengths promotes one-electron base oxidation. Biologically, Fenton chemistry and hydroxyl radicals can cause base damage (*27*, *28*). Significantly, some pathways that generate base lesions such as 8-oxodeoxyguanosine may not involve direct collision with the base but instead charge transport at long range to promote base oxidation.

We see with Rh reaction and photolysis at high versus low energies where these damage sites occur and where oxidative damage is funneled. Just as we observed with purified mtDNA, one-electron oxidative damage is funneled to sites in conserved sequence block II, sites that are critical for mt replication. Moreover, these sites, positions 260 and 298, are closely aligned with germline and somatic mutations detected in mt from tumors (*7*, *8*, *29*). Position 298 flanks conserved sequence block II, which regulates the transition from transcription to DNA replication (*30*). Positioning guanosine-rich sequences in conserved sequence block II gives a simple and efficient strategy for the cell to repress the replication of oxidatively damaged DNA. As we previously hypothesized (*13*), DNA base oxidation at conserved sequence block II should decrease the ability of damaged mitochondrial genomes to be replicated. This work may thus illustrate such a check point for DNA damage in vivo.

Oxidative Damage Inhibits Protein−DNA Contacts. Strikingly, addition of piperidine to functioning mt causes primer extension stops that are localized not only within the control region but also at other far removed sites (Figure 3). Since removal of cellular protein by guanidinium chloride or proteinase K removes this stop pattern, the stop pattern must be protein-related. Likely, piperidine treatment denatures but retains the protein bound to DNA. These data thus appear to indicate that, within the mitochondria, proteins are bound at regular intervals along the duplex. Protein association with mtDNA has been documented, but the regularity of coverage has not been seen previously (*25*).

Interestingly, this coverage of the DNA by associated proteins does not inhibit long-range charge transport to effect damage. Just as we observe with the purified DNA, sites of oxidative damage are well-separated from Rh binding sites, and thus, oxidative damage must arise through a DNA-mediated reaction. It should be noted that little effect of protein binding on long-range DNA charge transport was evident also in studies of oxidative damage in nucleosomes (*21*).

Oxidative damage is seen here, however, to affect protein binding. This association of the DNA with protein cannot be considered simply a nonspecific, electrostatic coverage. Upon oxidation and base damage, the protein-related stops are decreased or lost, and this occurs without the local binding of Rh. It is therefore not Rh binding that inhibits protein association. Instead, we infer that base oxidation itself alters protein binding. Thus, with oxidative damage, the mtDNA is altered not only by the generation of an oxidative lesion but also by a corresponding change in protein−DNA contacts. In this way, the mtDNA damage is also identified by the mt protein machinery.

SUPPORTING INFORMATION AVAILABLE

Experiments that show proteinase K treatment of mitochondrial DNA followed by primer extension. This material is available free of charge via the Internet at http://pubs.acs.org.

REFERENCES

1. Wallace, D. C. (2005) A Mitochondrial, paradigm of metabolic, and degenerative diseases, aging, and cancer: a dawn for evolutionary medicine, *Annu. Rev. Biochem. 39*, 359−407.
2. Penta, J. S., Johnson, F. M., and Wachsman, J. T. (2001) and Copeland, W. C., Mitochondrial DNA in human malignancy, *Mutat. Res. 488*, 119−133.
3. Dang, C. V., and Semenza, G. L. (1999) Oncogenic alterations of metabolism, *Trends Biochem. Sci. 24*, 68−72.
4. Fliss, M., Usadel, H., Caballero, O. L., Wu, L., Buta, M. R., Eleff, S. M., and Jen, J., and Sidransky, D. (2000) Facile detection of mitochondrial DNA mutations in tumors and bodily fluids, *Science 287*, 2017−2019.
5. Parrella, P., Xiao, Y., Fliss, M., Sanchez-Cepedes, M., Mazzarelli, P., Rinaldi, M., Nicol, T., Gabreilson, E., Cuomo, C., and Cohen, D., *et al.* (2001) Detection of mitochondrial DNA mutations in primary breast cancer and fine-needle aspirates, *Cancer Res. 9*, 7623−7626.
6. Kang, D., and Hamasaki, N. (2005) Alterations of mitochondrial DNA in common diseases and diseased states: aging, neurodegeneration, heart failure, diabetes, and cancer, *Curr. Med. Chem. 12*, 429−441.
7. Kurtz, A., Lueth, M., Kluwe, L., Zhang, T., Foster, R., Mautner, V. F., Hartmann, M., Tan, D. J., Martuza, R. L., and Friedrich, R. E., *et al.* (2004) Somatic mitochondrial DNA mutations in neurofibromatosis type 1-associated tumors, *Mol. Cancer Res. 2*, 433−441.
8. Tan, D.-J., Bai, R.-K., and Wong, L. J. (2002) Comprehensive, scanning of somatic mitochondrial DNA mutations in breast cancer, *Cancer Res. 62*, 972−976.
9. de Souza-Pinto, N. C., Eide, L., Hogue, B. A., Thybo, T., Stevnsner, T., Seeberg, E., and Klungland, A. and Bohr, V. A. (2001) Repair of 8-oxodeoxyguanosine lesions in mitochondrial DNA depends on the oxoguanine DNA glycosylase (OGG1) gene and 8-oxoguanine accumulates in the mitochondrial DNA of OGG1-defective mice, *Cancer Res. 61*, 5378−5381.
10. Hsu, G. W., Ober, M., Carell, T. and Beese, L. S. (2004) Error-prone replication of oxidatively damaged DNA by a high-fidelity DNA polymerase, *Nature 431*, 217−221.
11. Rodriguez, H., Akman, S. A., Holmquist, G. P., Willson, G. L., and Driggers, W. J. and LeDoux, S. P. (2000) Mapping oxidative DNA damage using ligation mediated polymerase chain reaction technology, *Methods 22*, 148−156.
12. Vermulst, M., Bielas, J. H., Kujoth, G. C., Ladiges, W. C., Rabinovitch, P. S., and Prolla, T. A., and Loeb, L. A. (2007) Mitochondrial point mutations do not limit the natural lifespan of mice, *Nat. Genet. 39*, 540−543.
13. Merino, E. J., and Barton, J. K. (2007) Oxidation by DNA charge transport damages conserved sequence block II, a regulatory element in mitochondrial DNA, *Biochemistry 46*, 2805−2811.
14. Sitlani, A., and Barton, J. K. (1994) Sequence-specific recognition of DNA by phenanthrenequinone diimine complexes of rhodium-(III): importance of steric and van der Waals interactions, *Biochemistry 33*, 12100−12108.
15. Kielkopf, C. L., Erkkila, K. E., Hudson, B. P., and Barton, J. K. (2000) and Rees, D. C., Structure of a photoactive rhodium complex intercalated into DNA, *Nat. Struct. Biol. 7*, 117−121.
16. Hall, D. B., and Holmlin, R. E., and Barton, J. K. (1996) Oxidative DNA damage through long-range electron transfer, *Nature 382*, 731−735.
17. Saito, I., Takayama, M., and Sugiyama, H., and Nakatani, K. (1995) Photoinduced DNA cleavage via electron transfer: dem-

onstration that guanine residues located 5′ to guanine are the most electron-donating sites, *J. Am. Chem. Soc. 117*, 6406−6407.
18. Delaney, S., and Barton, J. K. (2003) Long-range DNA charge transport, *J. Org. Chem. 68*, 6475−6483.
19. O'Neill, M. A., and Barton, J. K. (2004) DNA-mediated charge transport chemistry and biology, *Top Curr. Chem. 236*, 67−115.
20. Nunez, M. E., and Hall, D. B., and Barton, J. K. (1998) Long-range oxidative damage to DNA: effects of distance and sequence, *Chem. Biol. 6*, 85−97.
21. Nunez, M. E., and Noyes, K. T., and Barton, J. K. (2002) Oxidative charge transport through DNA in nucleosome core particles, *Chem. Biol. 9*, 403−415.
22. Bjorklund, C. C., and Davis, W. B. (2006) Attenuation of DNA charge transport by compaction into a nucleosome core particle, *Nucleic Acids Res. 34*, 1836−1846.
23. Nunez, M. E., and Holmquist, G. P., and Barton, J. K. (2001) Evidence for DNA charge transport in the nucleus, *Biochemistry 40*, 12465−12471.
24. Garcia-Ruiz, C., Colell, A., Mari, M., and Morales, A., and FernandezCheca, J. C. (1997) Direct effect of ceramide on the mitochondrial electron transport chain leads to generation of reactive oxygen species−Role of mitochondrial glutathione, *J. Biol. Chem. 272*, 11369−11377.
25. Bogenhagen, D. F., Wang, W., and Shen, E. L., and Kobayashi, R. (2003) Protein components of mitochondrial DNA nucleoids in higher eukaryotes, *Mol. Cell Proteomics 2*, 1205−1216.
26. Reers, M., and Smith, T. W., and Chen, L. B. (1991) J-aggregate formation of a carbocyanine as a quantitative fluorescent indicator of membrane potential, *Biochemistry 30*, 4480−4486.
27. Burrows, C. J., and Muller, J. G. (1998) Oxidative nucleobase modifications leading to strand scission, *Chem. Rev. 98*, 1109−1151.
28. Wagenknecht, H.-A. (2006) Electron transfer processes in DNA: mechanisms, biological relevance and applications in DNA analytics, *Nat. Prod. Rep. 23*, 973−1006.
29. Wang, Y., Michikawa, Y., Mallidis, C., Bai, Y., Woodhouse, L., Yarasheski, K. E., Miller, C. A., Askanas, V., Engel, W. K., Bhasin, S., et al. (2001) Muscle-specific mutations accumulate with aging in critical human mtDNA control sites for replication, *Proc. Natl. Acad. Sci. U.S.A. 98*, 4022−4027.
30. Xu, B., and Clayton, D. A. (1996) RNA-DNA hybrid formation at the human mitochondrial heavy-strand origin ceases at replication start sites: and implication for RNA-DNA hybrids serving as primers, *EMBO J. 15*, 3135−3143.

BI701775S